

SCIENTIFIC REPORTS



OPEN

Molecular pain markers correlate with pH-sensitive MRI signal in a pig model of disc degeneration

Maxim Bez^{1,2}, Zhengwei Zhou^{3,4}, Dmitriy Sheyn^{2,5,6,8}, Wafa Tawackoli^{2,3,5,6}, Joseph C. Giaconi⁷, Galina Shapiro¹, Shiran Ben David^{2,5}, Zulma Gazit^{1,2,5,8}, Gadi Pelled^{1,2,5,6}, Debiao Li^{3,4,7} & Dan Gazit^{1,2,3,5,6,8}

Intervertebral disc (IVD) degeneration is a leading cause of chronic low back pain that affects millions of people every year. Yet identification of the specific IVD causing this pain is based on qualitative visual interpretation rather than objective findings. One possible approach to diagnosing pain-associated IVD could be to identify acidic IVDs, as decreased pH within an IVD has been postulated to mediate discogenic pain. We hypothesized that quantitative chemical exchange saturation transfer (qCEST) MRI could detect pH changes in IVDs, and thence be used to diagnose pathologically painful IVDs objectively and noninvasively. To test this hypothesis, a surgical model of IVD degeneration in Yucatan minipigs was used. Direct measurement of pH inside the degenerated IVDs revealed a significant drop in pH after degeneration, which correlated with a significant increase in the qCEST signal. Gene analysis of harvested degenerated IVDs revealed significant upregulation of pain-, nerve- and inflammatory-related markers after IVD degeneration. A strong positive correlation was observed between the expression of pain markers and the increase in the qCEST signal. Collectively, these findings suggest that this approach might be used to identify which IVD is causing low back pain, thereby providing valuable guidance for pain and surgical management.

Low back pain is one of the most frequent causes of morbidity and disability¹. It occurs most often in humans between 30 and 50 years of age due to the aging process, but also happens as a result of genetic predisposition, mechanical injuries, and a sedentary life style^{2,3}. Americans spend at least 50 billion dollars each year on low back pain, the most common cause of job-related disability and a leading contributor to missed work⁴. Intervertebral disc (IVD) degeneration is believed to be a major source of chronic low back pain, and more than 90% of surgical spine procedures are performed with the aim of relieving the consequences of this degenerative process⁵. Current diagnostic approaches include computerized tomography (CT) and magnetic resonance imaging (MRI), which provide detailed soft tissue imagery but thus far fail to differentiate between a pathologically painful disc and a physiologically aging disc that does not generate pain^{6,7}. Due to the shortcomings of these imaging studies, new diagnostic methods that rely on other biomarkers are being developed for low back pain.

In adults, the IVD is avascular; its nutrition depends on diffusion via the annulus fibrosus and adjacent vertebral endplates⁸. Typically, nucleus pulposus cells obtain energy by anaerobic glycolysis, leading to the production of lactic acid, which is then expelled from the IVD by diffusion. In IVDs that have degenerated due to changes in blood supply in the region, sclerosis of the subchondral bone, or endplate calcification, the supply of glucose and clearance of lactate decreases, thereby leading to a sharp drop in pH^{9,10}. The pH of human IVDs ranges from 7.1 in healthy IVDs to lower than 6 in degenerated IVDs^{11,12}. Therefore, a recent hypothesis was made that low pH values within the degenerated IVDs are the cause of discogenic low back pain^{13,14}.

¹Skeletal Biotech Laboratory, Faculty of Dental Medicine, The Hebrew University of Jerusalem, Ein Kerem, 91120, Jerusalem, Israel. ²Department of Surgery, Cedars-Sinai Medical Center, Los Angeles, CA, 90048, USA. ³Biomedical Imaging Research Institute, Cedars-Sinai Medical Center, Los Angeles, 90048, CA, USA. ⁴Department of Bioengineering, University of California Los Angeles, Los Angeles, California, USA. ⁵Board of Governors Regenerative Medicine Institute, Cedars-Sinai Medical Center, Los Angeles, CA, 90048, USA. ⁶Department of Biomedical Sciences, Cedars-Sinai Medical Center, Los Angeles, CA, 90048, USA. ⁷Department of Imaging, Cedars-Sinai Medical Center, Los Angeles, CA, 90048, USA. ⁸Department of Orthopedics, Cedars-Sinai Medical Center, Los Angeles, CA, 90048, USA. Maxim Bez and Zhengwei Zhou contributed equally. Correspondence and requests for materials should be addressed to D.G. (email: Dan.Gazit@csmc.edu)

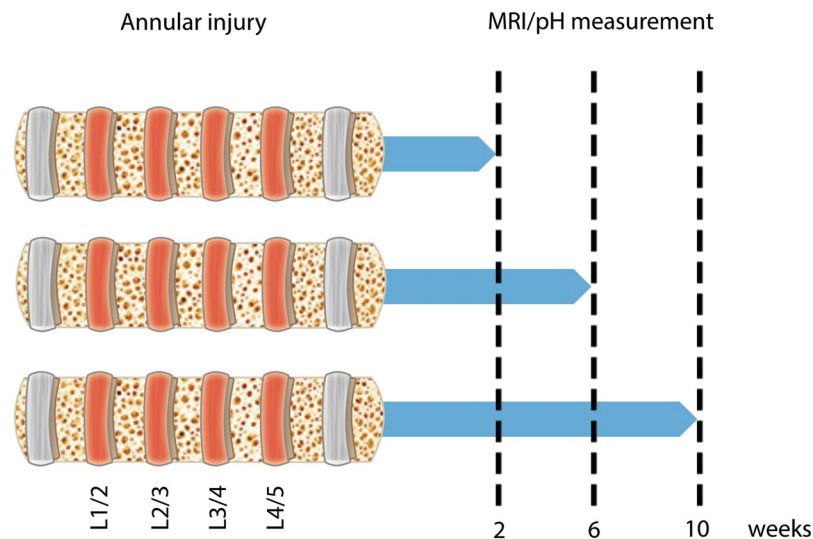


Figure 1. IVD degeneration timeline. Annular injuries were created in four IVD levels in minipigs to induce disc degeneration (depicted in red). Following this procedure, the animals were randomly divided into 3 groups (3 animals in each group) and imaged at 2, 6, and 10 weeks. At each time point, the animals in one group were sacrificed and the pH within their injured IVDs was measured. The IVDs were harvested for gene expression, histological, and immunohistofluorescence analyses.

Recent advances in MRI technologies have allowed researchers to noninvasively assess pH changes in the body. Of particular note, chemical exchange saturation transfer (CEST) has been studied to measure pH-dependent MRI signal changes^{15–18}. This technique exploits the chemical exchange, which is pH sensitive, between water protons and solute protons in certain molecules. Previous studies have applied CEST to detect pH changes in IVDs in pigs¹⁹ and humans²⁰. However, the CEST signal can be affected by other contributing factors, including water relaxation parameters and solute concentration²¹. To eliminate these confounding factors, quantitative CEST (qCEST) was developed to measure the exchange rate, independently from T_1 and T_2 signals as well as from the solute concentration^{22–25}. In the nucleus pulposus, glycosaminoglycans' (GAGs') hydroxyl protons can serve as an endogenous agent for qCEST to measure the pH-sensitive exchange rate with water protons. It has recently been shown that the exchange rate measured using qCEST is closely correlated to pH values found in the IVD²⁶.

In this study, we hypothesized that discogenic pain is caused by a drop in pH within the degenerating IVD and thus can be detected using qCEST in a clinically relevant, large animal model of IVD degeneration. Changes in the expression profile of several pain markers, as they relate to degenerative processes and changes in pH within the IVD, were also examined *in vivo*.

Results

Induction of IVD degeneration. Minipigs underwent surgery during which the annulus fibrosus of four lumbar IVDs (L1/2, L2/3, L3/4, L4/5) was punctured to induce disc degeneration (Fig. 1). The progress of IVD degeneration was then monitored using a clinical 3T MRI system (Fig. 2A). T_2 values following injury were significantly reduced at all time points compared to healthy porcine IVDs, suggesting loss of water content ($p < 0.0001$; Fig. 2B). The T_2 values were further reduced 10 weeks after IVD puncture compared to Week 2 ($p < 0.05$). In addition, a significant reduction in the T_1 signal from 1.6 to 1.4 was noticeable 2 weeks after puncture compared to the signal in healthy controls ($p < 0.0001$; Fig. 2C). A further reduction in the T_1 signal to 1.2 was measured 6 weeks after IVD puncture ($p < 0.0001$). $T_{1\rho}$ mapping revealed a two-fold reduction as early as 2 weeks after injury ($p < 0.0001$; Fig. 2D). Overall, these quantitative MR signals revealed a rapidly progressive degenerative status of the punctured IVDs^{27,28}. Histology (Fig. 2E) and microphotography (Fig. S1) revealed an abnormal IVD structure and extracellular matrix following puncture of the annulus fibrosus, with extensive fibrosis and formation of cell clusters in the nucleus pulposus, which is typical of degenerated IVDs²⁹.

MR signal correlates with intradiscal pH in degenerated IVDs. In addition to characterizing the degenerative status of IVDs based on T_2 , T_1 , and $T_{1\rho}$ signals, we acquired qCEST signals (represented as the exchange rate k_{sw} between water protons and GAG protons) from the degenerated IVDs (Fig. 3A). A significant drop in pH from 7.2 to 6.3 was found in IVDs as soon as 2 weeks after injury and this drop continued until Week 10 ($p = 0.0001$, Fig. 3B). The qCEST signal significantly increased 2 weeks after injury ($p < 0.05$, Fig. 3C) and further increased at 6 and 10 weeks ($p < 0.01$). A strong correlation was observed between the qCEST signal and the direct pH reading across all time points (Fig. 3D, $k_{sw} = 1.3 \times 10^{-\text{pH}+8} + 248.2$, $R^2 = 0.8004$; $p < 0.0001$). In addition, a receiver operating characteristics (ROC) analysis indicated that qCEST measurements could be used to differentiate between healthy and degenerated IVDs with 81.3% sensitivity and 76.1% specificity (Fig. S2, area under the curve = 0.813, $p = 0.0003$).

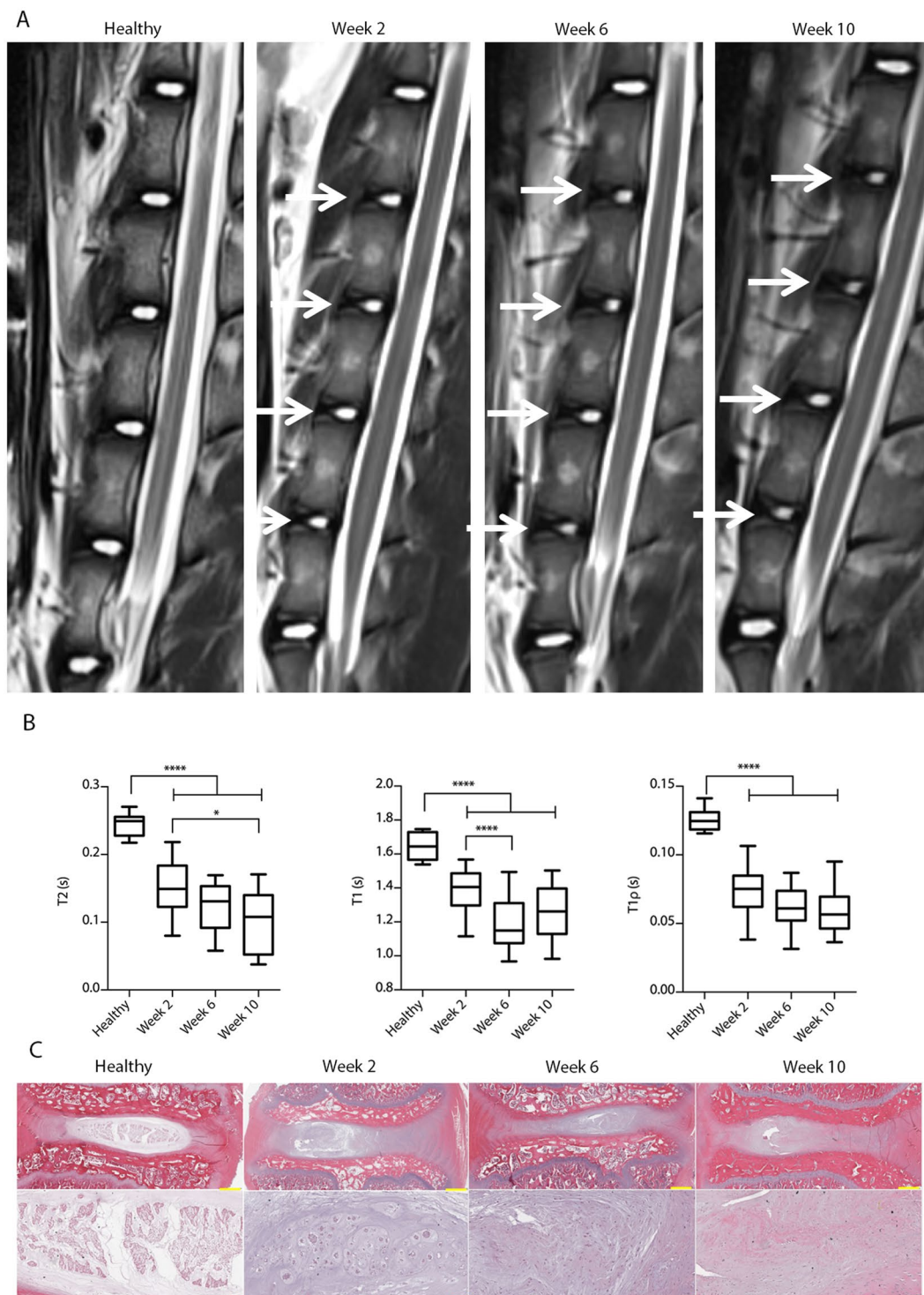


Figure 2. IVD degeneration following intradiscal puncture. **(A)** The progress of IVD degeneration at 2, 6, and 10 weeks following intradiscal puncture, as monitored by T_2 -weighted sagittal MRI. White arrows denote the degenerated IVDs. Quantification of **(B)** T_2 , **(C)** T_1 , and **(D)** $T_{1\rho}$ mappings of degenerated IVDs compared to healthy controls at 2, 6, and 10 weeks after puncture ($n = 12$ per experimental group; $*p < 0.05$, $***p < 0.0001$). **(E)** Hematoxylin and eosin staining of representative degenerated IVDs 2, 6, and 10 weeks after intradiscal puncture; microphotographs are shown at both low (upper subfigures; scale bars = 1 mm) and high (lower subfigures; scale bars = 100 μm) magnifications.

MR signal correlates with pain markers in degenerated IVDs. Next, we evaluated the expression of pain-related genes in the degenerated IVDs. Specifically, we evaluated the expression of calcitonin gene-related peptide (*CGRP*), bradykinin receptor B1 (*BDKRB1*), and catechol-*O*-methyltransferase (*COMT*). The earliest

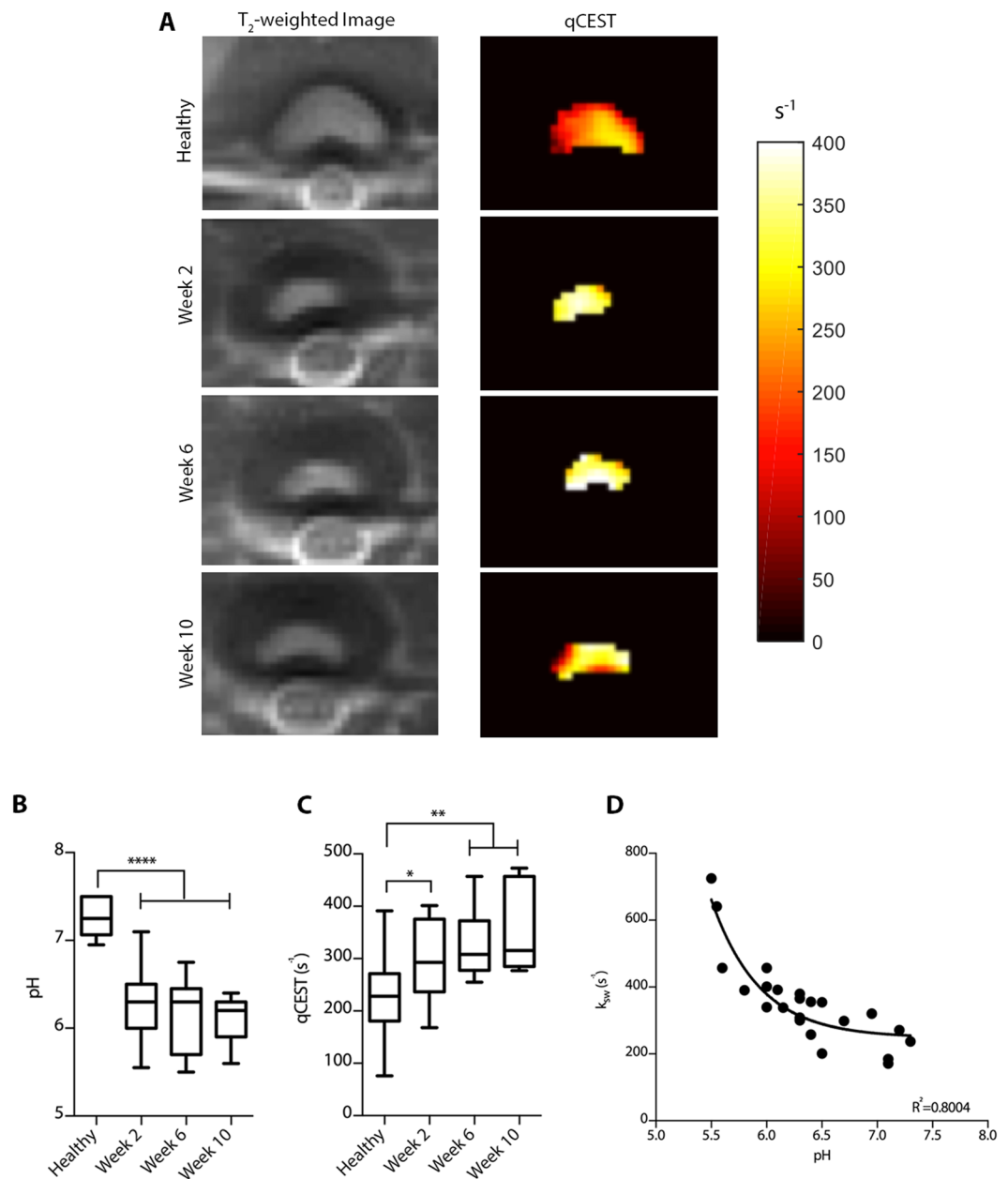


Figure 3. pH and qCEST changes following IVD degeneration. **(A)** Representative axial anatomical images of IVDs and their corresponding qCEST heat maps. **(B)** pH and **(C)** qCEST measurements within the degenerating IVDs at 2, 6, and 10 weeks after intradiscal puncture. **(D)** Correlation between the qCEST signal, represented by the exchange rate between the solute pool and the water pool (k_{sw}), and the pH measured within the IVD following animal sacrifice ($n = 12$ per experimental group; * $p < 0.05$, ** $p < 0.01$, **** $p = 0.0001$; qCEST = quantitative chemical exchange saturation transfer).

gene to display significant upregulation was *COMT* at Week 2 at the annulus fibrosus of the degenerated IVD ($p < 0.01$, Fig. 4C). By Week 6, there was a significant upregulation of all pain markers (BDKRB1 and *COMT* at the annulus fibrosus, CGRP at the nucleus pulposus, $p < 0.05$, Fig. 4A–C). Finally, in Week 10 only CGRP expression was significantly enhanced ($p < 0.05$, Fig. 4A). The inflammation marker *IL-6* was increased 20-fold at 6 and 10 weeks after IVD puncture at the annulus fibrosus ($p < 0.05$, Fig. 4D). In addition, brain-derived neurotrophic factor (*BDNF*), which is involved with nerve growth, was only significantly upregulated at 6 weeks after injury in the annulus fibrosus and at 10 weeks in the nucleus pulposus ($p < 0.05$, Fig. 4E).

Immunofluorescent staining of the nucleus pulposus revealed increased protein expression and colocalization of pain markers in degenerated IVDs compared to healthy IVDs (Fig. 5). Co-localization of *COMT* and *IL-6* was observed within the degenerated IVDs (Fig. S3). Finally, strong linear correlations between qCEST signals and expression levels from both the nucleus pulposus and annulus fibrosus of CGRP ($R^2 = 0.8758$, $p < 0.0001$), BDKRB1 ($R^2 = 0.8623$, $p < 0.0001$), *COMT* ($R^2 = 0.9025$, $p < 0.0001$), *IL-6* ($R^2 = 0.8368$, $p < 0.0001$), and

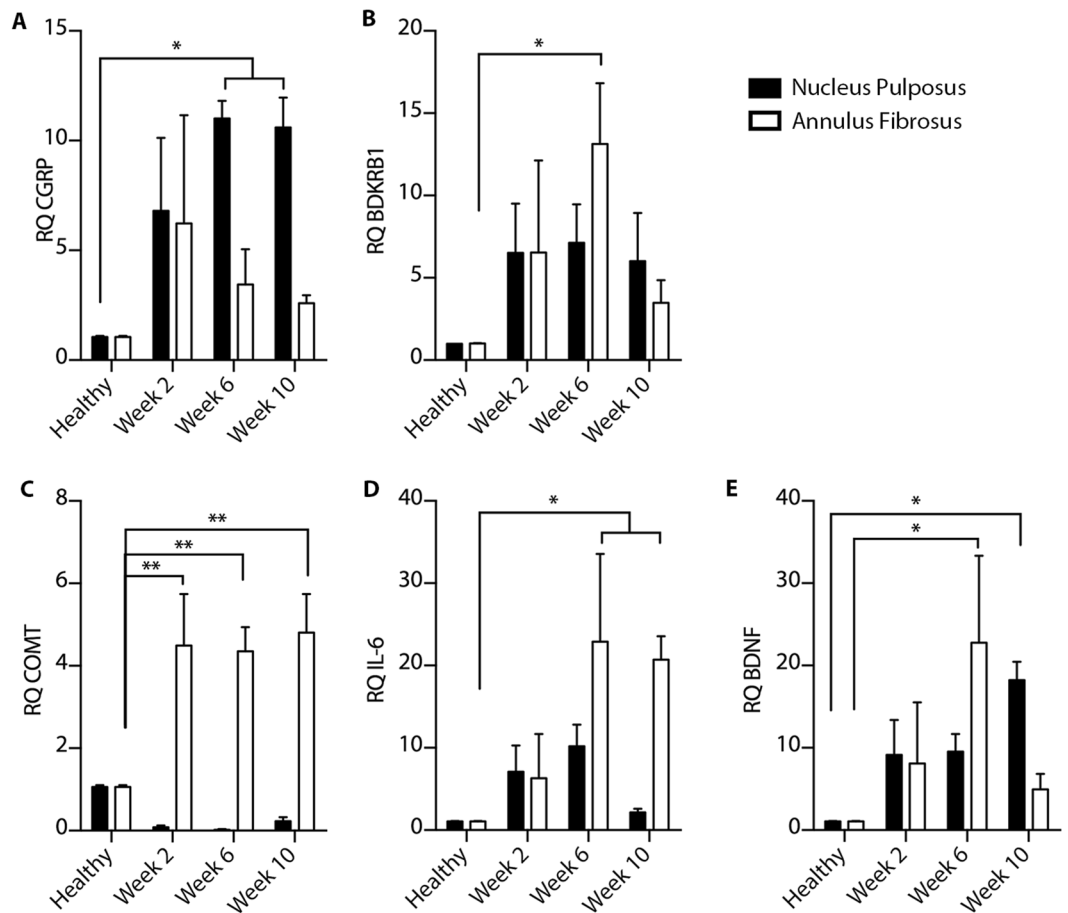


Figure 4. Upregulation of pain and inflammatory markers in degenerating IVDs. Quantitative RT-PCR analyses of (A–C) pain-related genes (CGRP, BDKRB1 and COMT) and (D,E) inflammation-related genes (IL-6 and BDNF) harvested from healthy and degenerated IVDs 2, 6, and 10 weeks after intradiscal puncture (n = 3 per group; *p < 0.05, **p < 0.01; RQ, relative quantification, CGRP, calcitonin gene-related peptide, BDKRB1, bradykinin receptor B1, COMT, catechol-*O*-methyltransferase, BDNF, brain-derived neurotrophic factor).

BDNF ($R^2 = 0.9219$, $p < 0.0001$) were observed (Fig. 6). Combined, these results show that the qCEST signal is anti-correlated with pH and correlated with pain and inflammatory markers within the IVDs.

Discussion

In this study, we used MRI to detect intradiscal pH changes that correlated with upregulation of pain markers in a minipig model of IVD degeneration. We showed that disc degeneration was achieved by 10 weeks following IVD puncture, as detected by MRI and histology. A significant drop in pH was observed during the degenerative process as well as a significant increase in the qCEST signal. These changes were detected as early as 2 weeks after injury. The qCEST signals were anti-correlated with pH measurements obtained directly from the degenerated IVDs. Gene analysis revealed upregulation of pain markers in degenerated IVDs—a finding that was strongly correlated with the qCEST signal at various time points.

Quantitative MR sequences offer new objective markers capable of differentiating healthy and injured IVDs. Conventional quantitative protocols of T_1 - and T_2 -relaxation times, and more recently $T_{1\rho}$ mapping, are well established in the literature as proxies for the detection of pathological changes within IVDs^{6,30–33}. Of particular interest, the $T_{1\rho}$ signal has been compared to findings of lumbar provocative discography as a quantitative biomarker of low back pain³⁴. In that study, researchers demonstrated that loss of proteoglycans, as shown by a reduced $T_{1\rho}$ signal, can be used to detect painful IVDs with a moderate correlation to discography. However, these results most likely stem from the relatively low specificity of the method, as the loss of proteoglycans is a common feature of IVD degeneration and does not necessarily correlate to pain symptoms³⁵. In addition, performing the discography procedure immediately before MRI raises the question of whether the injection of a contrast agent affects the measured $T_{1\rho}$ signal within the IVD due to increased water content.

Newer methods in which gagCEST protocols are used to evaluate GAG content have also been tested to detect low back pain. Wada *et al.* showed that there is a correlation between the gagCEST signal and the Pfirrmann score in patients with low back pain ($r = -0.675$)³⁶. A similar work, in which the same approach was used, showed a weaker correlation in patients ($r = -0.449$)³⁷. While no direct correlation to pain scoring was shown in either work, the gagCEST signal depends on the T_1 and T_2 signals, and the collagen content, making this approach less

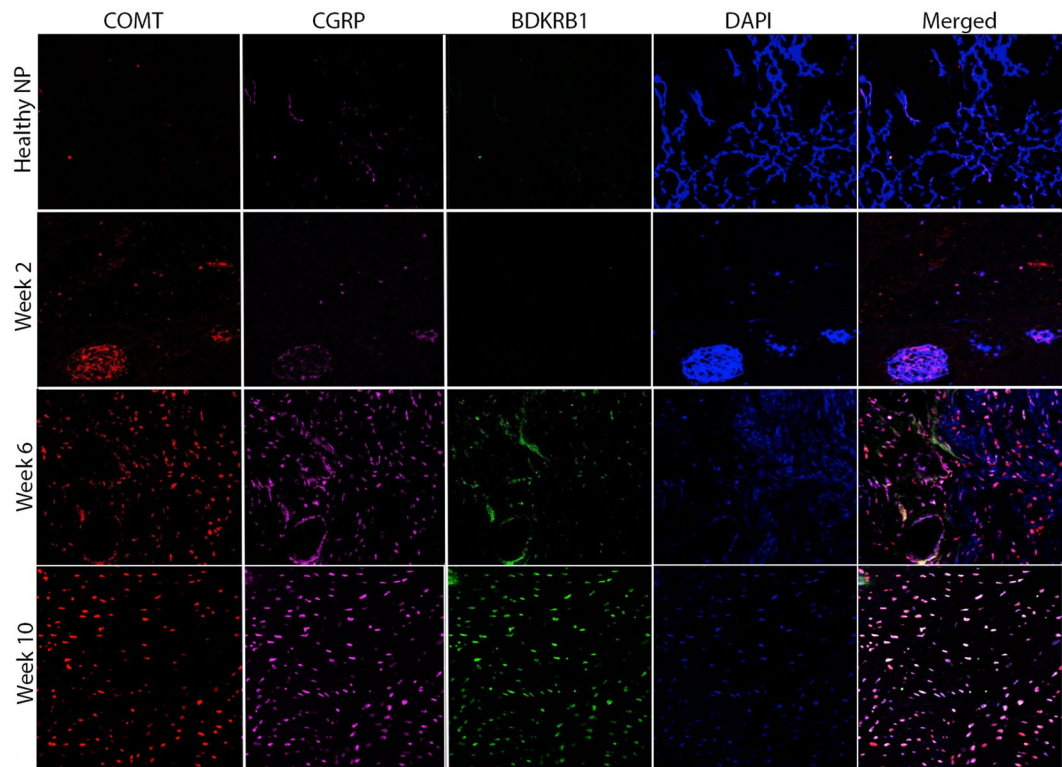


Figure 5. Immunofluorescence of pain-related marker upregulation. Microphotographs showing IVD tissue samples after immunostaining against COMT, CGRP, and BDKRB1, and counterstaining with DAPI; the samples were examined 2, 6, and 10 weeks after intradiscal puncture. Merged panels of the various stains are presented in the right column (NP = nucleus pulposus, CGRP = calcitonin gene-related peptide, BDKRB1 = bradykinin receptor B1, COMT = catechol-*O*-methyltransferase).

reliable^{20,21,38}. Although loss of GAGs occurs early in the degenerative process of IVDs and can therefore be used as an early marker of IVD degeneration³⁵, no causative relationship has been shown between depletion of GAGs and discogenic low back pain.

In addition to GAG loss, disc acidification has been implicated in discogenic pain development. This process could irritate locally infiltrating nerve fibers, thereby triggering discogenic pain. Several publications have shown that cells isolated from degenerated IVDs overexpress and secrete several pain-related and neurotrophic factors that enhance nerve growth, including BDNF and nerve growth factor^{39–41}. In addition, conditioned medium from degenerate IVD cells promote increased neurite outgrowth in nerve cells³⁹. There is evidence that in degenerative IVDs, the number of nerve fibers at the outer layer of the annulus fibrosus increases and nerve fibers grow into inner portions of the annulus and, occasionally, even into the nucleus pulposus—areas that otherwise are not innervated in healthy individuals^{42–44}.

In the pig disc degeneration model, we studied changes in gene expression of pain and inflammatory markers both in the nucleus pulposus and the annulus fibrosus. Our findings showed that pain markers were upregulated within the annulus fibrosus as soon as 2 weeks after injury, followed by pain marker upregulation at both locations. We also observed overexpression of BDNF in the annulus fibrosus 6 weeks after the injury; this was followed by expression of BDNF in the nucleus pulposus at 10 weeks. These patterns of expression concur with reports of nerve fiber penetration into the nucleus pulposus. A recent study showed that acidic pH directly causes an increase in several pro-inflammatory, neurotrophic, and pain-related factors in cultured human nucleus pulposus cells, including IL-6 and BDNF, in a similar fashion to our findings⁴⁵. This upregulation may be responsible for the ingrowth of nerve fibers into degenerate IVDs, and low pH is a contributing factor to this process.

Furthermore, acid-sensing ion channels (ASICs), extracellular receptors that respond to a low pH, were found to be upregulated after exposure to an acidic environment in nucleus pulposus cells and to regulate the biological activity of these cells^{46–48}. ASIC3 was found to protect IVD cells from apoptosis in low pH conditions⁴⁸. In the same study, it was shown that nerve growth factor is required to maintain a basal level of ASIC3; thus, it is conceivable that IVD cells secrete nerve growth factor to protect themselves from an acidic environment within the IVD and indirectly activate pain fibers in this process. Researchers have inhibited the activity of ASICs in nucleus pulposus cells, showing a reduction in the expression of pro-inflammatory, neurotrophic, and pain-related factors in an acidic environment^{45,49}. Although the exact mechanism underlying these processes remains elusive, these findings indicate a close relationship between low pH and discogenic pain.

One of the biggest challenges in using animals to study IVD degeneration relates to pain perception. Gruber *et al.* conducted a genome-wide analysis of IVD specimens from human patients to examine key pain-related genes

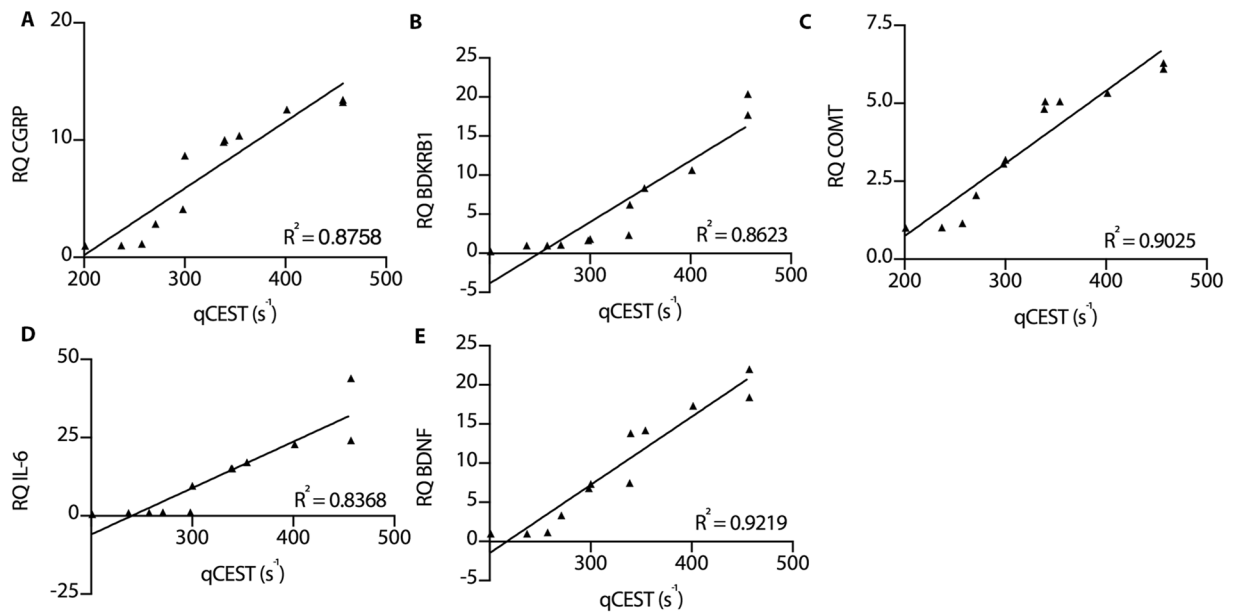


Figure 6. Linear correlation between qCEST and biomarkers in degenerating IVDs. Correlation plots between qCEST signal and expression levels of (A) CGRP, (B) BDKRB1, (C) COMT, (D) IL-6, and (E) BDNF extracted from degenerated and healthy annulus fibrosus and nucleus pulposus (RQ, relative quantification).

associated with discogenic pain⁵⁰. Similar to our findings, these researchers' work showed upregulation of CGRP, COMT, and BDKRB1 in pathological IVD specimens; this was confirmed by positive immunohistochemical staining in the annulus. These pain-related factors could mediate hyperalgesia in chronic inflammation⁵¹, stimulate sensory nerves in inflamed tissues⁵², and participate in the metabolism of pain neurotransmitters, including noradrenalin, adrenaline, and dopamine⁵³. CGRP upregulation was also observed in an acute injury model of the IVD in a neurotrophic gene expression-dependent manner⁵⁴. Thus, our findings could serve as a biological clue that our degeneration model causes discogenic pain in experimental animals.

Other previous studies attempted to evaluate pH as a biomarker for diagnosing discogenic low back pain. Zuo *et al.* demonstrated the feasibility of acquiring localized ¹H spectra using a 3.0T imager in intact bovine and human cadaveric IVDs to quantify lactate causing low pH⁵⁵. Translating this technique to *in vivo* spectroscopy suffers from several limitations. As stated by the authors, it is difficult to differentiate lactate from lipid peaks because their resonance frequencies are close. Another limitation is inadequate quantification of metabolites in IVDs within the collapsed space. A later study from the same group characterized IVDs *in vivo* by using magnetic resonance spectroscopy (MRS)⁵⁶. A significantly elevated water/proteoglycan area ratio was found in IVDs identified as the source of pain by discography. *In vivo* MRS is challenging because of a low signal-to-noise ratio, physiological motion, and bone susceptibility-induced line broadening, making the assessment of lactate imprecise. Another study found a nonlinear dependence of the CEST effect of GAG on pH in porcine IVD specimens¹⁹. However, that study was performed *ex vivo* using a 7.0T MRI unit, which currently is not widely available in the clinical setting.

While we observed the animals for up to 10 weeks after IVD puncture, the subclinical degenerative processes in humans can take many years. In this study, we observed in all injured IVDs a drop in pH with upregulation of several pain markers, which persisted for 10 weeks. A long-term study will probably be required to broaden the validity of this approach to include chronic IVD degeneration and differentiate between degenerated painful discs and degenerated nonpainful discs in humans.

Overall, these results show great promise for future human studies, as this approach can be easily and readily implemented using clinical MRI systems. qCEST protocols can be used to provide additional information on IVD physiology and to detect pH changes associated with early IVD degeneration, thus providing an early, noninvasive, and objective diagnosis that can be used to prompt early intervention and prevention of chronic low back pain.

Materials and Methods

Study design. The objective of our study was to develop a pH-level-based MRI approach to diagnose low back pain. Our prespecified hypothesis was that the acidic intradiscal environment that contributes to discogenic pain can be detected noninvasively using qCEST imaging. qCEST was investigated for its capacity to detect pH changes within IVDs and predict pain marker expression. Nine healthy female skeletally mature Yucatan minipigs (S&S Farms; average age 7 months, 35–40 kg) were included in this study. The sample size that we used was estimated to achieve a power of 0.8 and $\alpha = 0.05$ using one-way ANOVA. All animals underwent a surgical procedure in which multiple-level lumbar IVD degeneration was induced (Fig. 1). The degeneration was induced in the lumbar spine as it is the major source of low back pain since it is affected the most by age-related degenerative

processes⁵⁷. Afterward, the animals underwent MRI at 2, 6, and 10 weeks. At each time-point, three minipigs were randomly selected for euthanasia to directly measure the pH within the affected IVD as well as to analyze gene expression, histological architecture, and protein expression. IVD degeneration was evaluated based on imaging parameters and histological findings. Pain was detected based on gene expression and findings of immunofluorescence, and was compared to qCEST measurements within the IVDs. Animals that developed periprocedural complications, such as nerve damage or signs of distress, were eliminated from the study.

IVD degeneration animal model. All experiments using animals and procedures of animal care and handling were carried out in strict accordance with the recommendations of The Association for Assessment and Accreditation of Laboratory Animal Care. All animal procedures were approved by the Cedars-Sinai Medical Center institutional review board for animal experiments. A previously published IVD degeneration model⁵⁸ was adapted for this study. Briefly, following an 18-hr preoperative fast, each minipig was sedated using intramuscular acepromazine (0.25 mg/kg), ketamine (20 mg/kg), and atropine (0.02–0.05 mg/kg). The animal was then administered propofol (2 mg/kg) intravenously and endotracheal intubation was performed. Anesthesia was maintained using 1–3.5% inhaled isoflurane for the duration of the procedure. IVD degeneration was induced by a single annular injury as published elsewhere⁵⁹. Specifically, under fluoroscopic guidance, a 14-G VertePort needle (Stryker, Kalamazoo, MI) was used to penetrate and injure the annulus fibrosus of the IVD parallel to the endplate via a posterolateral approach. This procedure was repeated at four target levels: L1/L2, L2/L3, L3/L4, and L4/L5.

In vivo MRI. Imaging studies were performed using a 3T clinical MRI system (Magnetom Verio; Siemens Healthcare, Erlangen, Germany). Animals were placed in the right decubitus position with body array coils centered on lumbar spinous processes. CEST MRI, T₁, T₂ and T_{1ρ} mapping were performed in the axial plane for each IVD. Total scan time was approximately 40 minutes for each IVD.

CEST MRI was performed using a two-dimensional reduced field of view TSE CEST sequence (TR/TE = 10500/10 ms, 2 averages, single shot)⁶⁰. For each IVD, images were acquired in the axial plane with a slice thickness of 3 mm, a field of view of 140 × 40 mm², and a spatial resolution of 1.1 × 1.1 mm². The CEST saturation module consisted of 39 Gaussian-shaped pulses, with a duration t_p = 80 ms for each pulse and an interpulse delay t_d = 80 ms (duty cycle = 50%, total saturation duration T_s = 6240 ms) at saturation flip angles of 900, 1500, 2100, and 3000 [B₁ amplitudes = flip angle/(gt_p) = 0.73, 1.22, 1.71, and 2.45 μT]; the Z-spectrum was acquired with 10 different saturation frequencies at ±1.6, ±1.3, ±1.0, ±0.7, and ±0.4 ppm.

The B₀ field was corrected using a water saturation shift referencing (WASSR) map⁶¹ with the same imaging readout parameters. The CEST saturation module for WASSR map consisted of 2 Gaussian-shaped pulses, with a duration t_p = 30 ms for each pulse and an interpulse delay t_d = 30 ms (duty cycle = 50%, total saturation duration T_s = 120 ms) at saturation flip angles of 90°. The images were acquired from −0.8 ppm to 0.8 ppm with a step size of 0.2 ppm.

T₁ mapping was performed using an inversion recovery TSE sequence with seven different inversion times (TI = 50, 150, 350, 700, 1050, 1400, and 2000 ms), TR/TE = 6000/12 ms, FOV = 280 × 280 mm², and spatial resolution = 1.1 × 1.1 × 3 mm³.

T₂ mapping was performed using a TSE sequence with various echo delays (TE = 12, 25, 50, 99, 199, and 397 ms; TR = 6000 ms), FOV = 280 × 280 mm², and spatial resolution = 1.1 × 1.1 × 3 mm³.

T_{1ρ} mapping was performed using an rFOV TSE sequence with various spin lock times (TSL = 0, 10, 40, and 80 ms). A spin-lock frequency of 300 Hz was used with TR/TE = 3500/9.1 ms, 1 average, FOV = 140 × 40 mm², and spatial resolution = 1.1 × 1.1 × 3 mm³.

MRI data analysis. Imaging data analysis was performed with custom-written programs in MATLAB (MathWorks, Natick, Massachusetts, USA) as previously reported²⁶.

The inverse CEST difference (CESTR_{ind}) was calculated for each B₁ amplitude using the following equation. Z_{+1.0 ppm} and Z_{−1.0 ppm} are the normalized signal intensity acquired at +1.0 ppm and −1.0 ppm after B₀ correction respectively.

$$\frac{1}{\text{CESTR}_{\text{ind}}} = \frac{1}{\frac{1}{Z_{+1.0 \text{ ppm}}} - \frac{1}{Z_{-1.0 \text{ ppm}}}}$$

As shown in the previous study²⁶, 1/CESTR_{ind} can be described as a linear function of 1/ω₁².

$$\frac{1}{\text{CESTR}_{\text{ind}}} \approx \frac{R_{1w}}{\text{DC} \cdot f_r \cdot k_{sw} \cdot c_1} + \frac{k_{sw} \cdot (R_{2s} + k_{sw}) \cdot R_{1w} \cdot c_2}{\text{DC} \cdot f_r \cdot k_{sw} \cdot c_1} \frac{1}{\omega_1^2}$$

where DC stands for duty cycle; c₁ and c₂ describe the shape of Gaussian saturation pulses (c₁ = σ√2π/t_p, c₂ = c₁√√2; σ and t_p are the width and length of the Gaussian pulse). ω₁ is defined as flip angle/pulse duration (in this study, 0.73, 1.22, 1.71, and 2.45 μT).

Linear regression was performed between 1/CESTR_{ind} and 1/ω₁² to estimate the slope *m* and intercept *n*, and eventually estimate k_{sw}.

$$k_{sw} = \frac{\sqrt{R_{2s}^2 + \frac{4m}{n \cdot c_2^2}} - R_{2s}}{2}$$

The T_1 maps were obtained by pixel-by-pixel least-squares fitting of the signal equation $I = I_0[1 - (1 + \eta) \cdot \exp(-TI/T_1)]$ where I is the signal intensity, TI is the inversion time and η is the inversion efficiency. The T_2 maps were obtained by fitting the signal equation $I = I_0 \cdot \exp(-TI/T_2)$ where I is the signal intensity and TE is the echo time. The $T_{1\rho}$ maps were obtained by fitting the signal equation $I = I_0 \cdot \exp(-TSL/T_{1\rho})$ where I is the signal intensity and TSL is the spin lock time.

IVD pH measurement. Intradiscal pH measurements were made immediately after animal sacrifice. A single pH value was obtained for each IVD. The spine was surgically exposed, and a custom-made needle-shaped tissue pH probe (Warner Instruments, Hamden, Connecticut, USA; Fig. S4) was inserted into the nucleus pulposus following a thin incision in the annulus fibrosus.

Gene expression analysis. Quantitative RT-PCR was performed on RNA extracted from degenerated IVDs harvested at 2, 6, and 10 weeks after induction of IVD degeneration and compared to control healthy discs. The expression of genes from degenerative IVDs was compared to healthy IVDs harvested from each time point. Total RNA was extracted from the annulus fibrosus and the nucleus pulposus by using the RNeasy Mini kit (Qiagen GmbH, Hilden, Germany) according to the manufacturer's protocol. RNA was retrotranscribed using random primers and reverse transcriptase (Promega Corp., Madison, WI, USA). Quantitative real-time PCR was performed using an ABI 7500 Prism system (Applied Biosystems, Foster City, CA). The expression of the following porcine genes was quantified: Bradykinin receptor B1 (BDKRB1; Ss03389804_s1, Thermo Fisher Scientific, Waltham, MA, USA), calcitonin gene-related peptide (CGRP; Ss03386432_uH) and catechol-O-methyltransferase (COMT; Ss04247881_g1), interleukin-6 (IL-6; Ss03384604_u1), and brain-derived neurotrophic factor (BDNF; Ss03822335_s1). Porcine 18 s was used as a housekeeping gene control.

Histological analysis and immunofluorescence imaging. Histological analysis was performed on degenerated IVDs harvested 2, 6, and 10 weeks after IVD puncture. The IVDs were sectioned and stained using hematoxylin and eosin, as previously described⁶². For immunofluorescent staining, the IVD tissues were deparaffinized, and the antigens were retrieved by incubation in preheated Target Retrieval Solution (Dako, Carpinteria, CA) for 45 min in 37 °C. Nonspecific antigens were blocked by applying blocking serum-free solution (Dako). Slides were stained with primary antibodies against BDKRB1, CGRP, COMT, IL-6, and BDNF (Table S1). The primary antibodies were applied to the slides, which were then incubated in 4 °C overnight. Then these antibodies were washed off using PBS, and the slides were incubated with a secondary antibody for 1 hr at room temperature, after which it also was washed off with PBS. Slides were then stained with 4',6-diamidino-2-phenylindole dihydrochloride (DAPI, 1 µg/ml) for 5 min in the dark, after which they were washed three times with PBS. A VectaMount mounting medium (Vector Laboratories, Burlingame, CA) was applied to the tissue. The slides were imaged using a 4-channel Laser Scanning Microscope 780 (Zeiss, Pleasanton, CA) with $\times 20$ magnification, z-stacking, and 5×5 tile scanning. For zoom-in images, a single z-stacked image was generated. All samples were scanned using the same gain and exposure settings.

Statistical analysis. GraphPad Prism 5.0 f software (GraphPad Prism, San Diego, CA) was used to analyze the data. Data analysis was conducted using one-way or two-way ANOVA with Tukey's multiple comparison post hoc test. Results are presented as means \pm SE. In box-and-whisker diagrams, the median is shown with a horizontal line, the box extends from the 25th to the 75th percentile, and the whiskers extend from the smallest value to the largest. Pearson correlation was performed between qCEST, pH, and RT-PCR values. ROC curve that depicts the diagnostic ability of qCEST to detect a true positive event of low back pain was generated for this study and the area under the curve was calculated. P values that were less than 0.05 were considered to be statistically significant.

Data and Materials Availability

All materials are available from commercial sources or can be derived using methods described in this study. All relevant data are reported in the article.

References

- Andersson, G. B. Epidemiological features of chronic low-back pain. *Lancet* **354**, 581–585 (1999).
- Knox, J. *et al.* The incidence of low back pain in active duty United States military service members. *Spine (Phila Pa 1976)* **36**, 1492–1500 (2011).
- Lefevre-Colau, M. M. *et al.* Frequency and interrelations of risk factors for chronic low back pain in a primary care setting. *PLoS One* **4**, e4874 (2009).
- Ascioglu, O., Gungorduk, K., Yildirim, G., Aslan, H. & Gunay, T. Maternal and perinatal outcomes of eclampsia with and without HELLP syndrome in a teaching hospital in western Turkey. *J Obstet Gynaecol* **34**, 326–331 (2014).
- An, H. S. *et al.* Introduction: disc degeneration: summary. *Spine (Phila Pa 1976)* **29**, 2677–2678 (2004).
- Majumdar, S., Link, T. M., Steinbach, L. S., Hu, S. & Kurhanewicz, J. Diagnostic tools and imaging methods in intervertebral disk degeneration. *Orthop Clin North Am* **42**, 501–511, viii (2011).
- Kang, C. H. *et al.* Can magnetic resonance imaging accurately predict concordant pain provocation during provocative disc injection? *Skeletal Radiol* **38**, 877–885 (2009).
- Raj, P. P. Intervertebral disc: anatomy-physiology-pathophysiology-treatment. *Pain Pract* **8**, 18–44 (2008).
- Menkin, V. Biochemical Mechanisms in Inflammation. *Br Med J* **1**, 1521–1528 (1960).
- Urban, J. P., Smith, S. & Fairbank, J. C. Nutrition of the intervertebral disc. *Spine* **29**, 2700–2709 (2004).
- Ichimura, K., Tsuji, H., Matsui, H. & Makiyama, N. Cell culture of the intervertebral disc of rats: factors influencing culture, proteoglycan, collagen, and deoxyribonucleic acid synthesis. *J Spinal Disord* **4**, 428–436 (1991).
- Nachemson, A. Intradiscal measurements of pH in patients with lumbar rhizopathies. *Acta Orthop Scand* **40**, 23–42 (1969).

13. Melkus, G., Grabau, M., Karampinos, D. C. & Majumdar, S. *Ex vivo* porcine model to measure pH dependence of chemical exchange saturation transfer effect of glycosaminoglycan in the intervertebral disc. *Magnetic resonance in medicine: official journal of the Society of Magnetic Resonance in Medicine/Society of Magnetic Resonance in Medicine* (2013).
14. Liang, C. Z. *et al.* The relationship between low pH in intervertebral discs and low back pain: a systematic review. *Arch Med Sci* **8**, 952–956 (2012).
15. Zhou, J., Payen, J. F., Wilson, D. A., Traystman, R. J. & van Zijl, P. C. Using the amide proton signals of intracellular proteins and peptides to detect pH effects in MRI. *Nat Med* **9**, 1085–1090 (2003).
16. Sun, P. Z. *et al.* Relaxation-compensated fast multislice amide proton transfer (APT) imaging of acute ischemic stroke. *Magn Reson Med* **59**, 1175–1182 (2008).
17. Sun, P. Z., Zhou, J., Sun, W., Huang, J. & van Zijl, P. C. Detection of the ischemic penumbra using pH-weighted MRI. *J Cereb Blood Flow Metab* **27**, 1129–1136 (2007).
18. Zhou, J. & van Zijl, P. C. Defining an Acidosis-Based Ischemic Penumbra from pH-Weighted MRI. *Transl Stroke Res* **3**, 76–83 (2011).
19. Melkus, G., Grabau, M., Karampinos, D. C. & Majumdar, S. *Ex vivo* porcine model to measure pH dependence of chemical exchange saturation transfer effect of glycosaminoglycan in the intervertebral disc. *Magn Reson Med* **71**, 1743–1749 (2014).
20. Liu, Q. *et al.* Detection of low back pain using pH level-dependent imaging of the intervertebral disc using the ratio of R1rho dispersion and -OH chemical exchange saturation transfer (RROC). *Magn Reson Med* **73**, 1196–1205 (2015).
21. Vinogradov, E., Sherry, A. D. & Lenkinski, R. E. CEST: from basic principles to applications, challenges and opportunities. *J Magn Reson* **229**, 155–172 (2013).
22. Wu, R., Xiao, G., Zhou, I. Y., Ran, C. & Sun, P. Z. Quantitative chemical exchange saturation transfer (qCEST) MRI - omega plot analysis of RF-spillover-corrected inverse CEST ratio asymmetry for simultaneous determination of labile proton ratio and exchange rate. *NMR Biomed* **28**, 376–383 (2015).
23. Sun, P. Z., Wang, Y., Dai, Z., Xiao, G. & Wu, R. Quantitative chemical exchange saturation transfer (qCEST) MRI-RF spillover effect-corrected omega plot for simultaneous determination of labile proton fraction ratio and exchange rate. *Contrast Media Mol Imaging* **9**, 268–275 (2014).
24. Wu, R., Longo, D. L., Aime, S. & Sun, P. Z. Quantitative description of radiofrequency (RF) power-based ratiometric chemical exchange saturation transfer (CEST) pH imaging. *NMR Biomed* **28**, 555–565 (2015).
25. Sun, P. Z., Xiao, G., Zhou, I. Y., Guo, Y. & Wu, R. A method for accurate pH mapping with chemical exchange saturation transfer (CEST) MRI. *Contrast Media Mol Imaging* **11**, 195–202 (2016).
26. Zhou, Z. *et al.* Quantitative chemical exchange saturation transfer MRI of intervertebral disc in a porcine model. *Magn Reson Med* **76**, 1677–1683 (2016).
27. Trattig, S. *et al.* Lumbar intervertebral disc abnormalities: comparison of quantitative T2 mapping with conventional MR at 3.0 T. *Eur Radiol* **20**, 2715–2722 (2010).
28. Auerbach, J. D. *et al.* *In vivo* quantification of human lumbar disc degeneration using T1rho-weighted magnetic resonance imaging. *Eur Spine J* **15**(Suppl 3), S338–344 (2006).
29. Zhao, C. Q., Wang, L. M., Jiang, L. S. & Dai, L. Y. The cell biology of intervertebral disc aging and degeneration. *Ageing Res Rev* **6**, 247–261 (2007).
30. Chatani, K., Kusaka, Y., Mifune, T. & Nishikawa, H. Topographic differences of 1H-NMR relaxation times (T1, T2) in the normal intervertebral disc and its relationship to water content. *Spine (Phila Pa 1976)* **18**, 2271–2275 (1993).
31. Chiu, E. J. *et al.* Magnetic resonance imaging measurement of relaxation and water diffusion in the human lumbar intervertebral disc under compression *in vitro*. *Spine (Phila Pa 1976)* **26**, E437–444 (2001).
32. Boos, N. *et al.* Tissue characterization of symptomatic and asymptomatic disc herniations by quantitative magnetic resonance imaging. *J Orthop Res* **15**, 141–149 (1997).
33. Blumenkrantz, G. *et al.* *In vivo* 3.0-tesla magnetic resonance T1rho and T2 relaxation mapping in subjects with intervertebral disc degeneration and clinical symptoms. *Magn Reson Med* **63**, 1193–1200 (2010).
34. Borthakur, A. *et al.* T1rho magnetic resonance imaging and discography pressure as novel biomarkers for disc degeneration and low back pain. *Spine (Phila Pa 1976)* **36**, 2190–2196 (2011).
35. Urban, J. P. & McMullin, J. F. Swelling pressure of the intervertebral disc: influence of proteoglycan and collagen contents. *Biorheology* **22**, 145–157 (1985).
36. Wada, T. *et al.* Glycosaminoglycan chemical exchange saturation transfer in human lumbar intervertebral discs: Effect of saturation pulse and relationship with low back pain. *J Magn Reson Imaging* **45**, 863–871 (2017).
37. Haneder, S. *et al.* Assessment of glycosaminoglycan content in intervertebral discs using chemical exchange saturation transfer at 3.0 Tesla: preliminary results in patients with low-back pain. *Eur Radiol* **23**, 861–868 (2013).
38. Kim, J., Wu, Y., Guo, Y., Zheng, H. & Sun, P. Z. A review of optimization and quantification techniques for chemical exchange saturation transfer MRI toward sensitive *in vivo* imaging. *Contrast Media Mol Imaging* **10**, 163–178 (2015).
39. Richardson, S. M. *et al.* Degenerate human nucleus pulposus cells promote neurite outgrowth in neural cells. *PLoS One* **7**, e47735 (2012).
40. Purmessur, D., Freemont, A. J. & Hoyland, J. A. Expression and regulation of neurotrophins in the nondegenerate and degenerate human intervertebral disc. *Arthritis Res Ther* **10**, R99 (2008).
41. Navone, S. E. *et al.* Expression of neural and neurotrophic markers in nucleus pulposus cells isolated from degenerated intervertebral disc. *J Orthop Res* **30**, 1470–1477 (2012).
42. Freemont, A. J. *et al.* Nerve ingrowth into diseased intervertebral disc in chronic back pain. *Lancet* **350**, 178–181 (1997).
43. Coppes, M. H., Marani, E., Thomeer, R. T., Oudega, M. & Groen, G. J. Innervation of annulus fibrosis in low back pain. *Lancet* **336**, 189–190 (1990).
44. Peng, B. *et al.* The pathogenesis of discogenic low back pain. *J Bone Joint Surg Br* **87**, 62–67 (2005).
45. Gilbert, H. T., Hodson, N., Baird, P., Richardson, S. M. & Hoyland, J. A. Acidic pH promotes intervertebral disc degeneration: Acid-sensing ion channel -3 as a potential therapeutic target. *Sci Rep* **6**, 37360 (2016).
46. Ohtori, S. *et al.* Up-regulation of acid-sensing ion channel 3 in dorsal root ganglion neurons following application of nucleus pulposus on nerve root in rats. *Spine (Phila Pa 1976)* **31**, 2048–2052 (2006).
47. Cuesta, A. *et al.* Acid-sensing ion channels in healthy and degenerated human intervertebral disc. *Connect Tissue Res* **55**, 197–204 (2014).
48. Uchiyama, Y. *et al.* Expression of acid-sensing ion channel 3 (ASIC3) in nucleus pulposus cells of the intervertebral disc is regulated by p75NTR and ERK signaling. *J Bone Miner Res* **22**, 1996–2006 (2007).
49. Liu, J. *et al.* Biological behavior of human nucleus pulposus mesenchymal stem cells in response to changes in the acidic environment during intervertebral disc degeneration. *Stem Cells Dev* (2017).
50. Gruber, H. E., Hoelscher, G. L., Ingram, J. A. & Hanley, E. N. Jr. Genome-wide analysis of pain-, nerve- and neurotrophin -related gene expression in the degenerating human annulus. *Mol Pain* **8**, 63 (2012).
51. Dray, A. & Perkins, M. Bradykinin and inflammatory pain. *Trends Neurosci* **16**, 99–104 (1993).
52. Donnerer, J., Schuligoi, R. & Stein, C. Increased content and transport of substance P and calcitonin gene-related peptide in sensory nerves innervating inflamed tissue: evidence for a regulatory function of nerve growth factor *in vivo*. *Neuroscience* **49**, 693–698 (1992).

53. Andersen, S. & Skorpen, F. Variation in the COMT gene: implications for pain perception and pain treatment. *Pharmacogenomics* **10**, 669–684 (2009).
54. Orita, S. *et al.* Inhibiting nerve growth factor or its receptors downregulates calcitonin gene-related peptide expression in rat lumbar dorsal root ganglia innervating injured intervertebral discs. *J Orthop Res* **28**, 1614–1620 (2010).
55. Zuo, J. *et al.* Assessment of intervertebral disc degeneration with magnetic resonance single-voxel spectroscopy. *Magn Reson Med* **62**, 1140–1146 (2009).
56. Zuo, J. *et al.* *In vivo* intervertebral disc characterization using magnetic resonance spectroscopy and T1rho imaging: association with discography and Oswestry Disability Index and Short Form-36 Health Survey. *Spine (Phila Pa 1976)* **37**, 214–221 (2012).
57. Kjaer, P., Leboeuf-Yde, C., Korsholm, L., Sorensen, J. S. & Bendix, T. Magnetic resonance imaging and low back pain in adults: a diagnostic imaging study of 40-year-old men and women. *Spine (Phila Pa 1976)* **30**, 1173–1180 (2005).
58. Mizrahi, O. *et al.* Nucleus pulposus degeneration alters properties of resident progenitor cells. *Spine J* **13**, 803–814 (2013).
59. Kim, K. S., Yoon, S. T., Li, J., Park, J. S. & Hutton, W. C. Disc degeneration in the rabbit: a biochemical and radiological comparison between four disc injury models. *Spine (Phila Pa 1976)* **30**, 33–37 (2005).
60. Liu, Q. *et al.* Reliable chemical exchange saturation transfer imaging of human lumbar intervertebral discs using reduced-field-of-view turbo spin echo at 3.0 T. *NMR Biomed* **26**, 1672–1679 (2013).
61. Kim, M., Gillen, J., Landman, B. A., Zhou, J. & van Zijl, P. C. Water saturation shift referencing (WASSR) for chemical exchange saturation transfer (CEST) experiments. *Magn Reson Med* **61**, 1441–1450 (2009).
62. Sheyn, D. *et al.* PTH promotes allograft integration in a calvarial bone defect. *Mol Pharm* **10**, 4462–4471 (2013).

Acknowledgements

We thank Edward Gill, Laura G. Smith, Hernan Rios, and Richard Tang for their help conducting the MRI acquisitions. NIH R01AR066517 (D.L., D.G.).

Author Contributions

G.P., Z.G., D.L. and D.G. contributed to the concept of the study and revised the manuscript. M.B., Z.Z., G.P. and D.G. designed the experiments. M.B., W.T. and J.C.G. performed large-animal surgical procedures. Z.Z. performed MRI acquisition and the imaging data analysis. M.B., W.T. and D.S. extracted the IVD tissue samples and performed pH measurements. M.B. and S.B.D. performed the RT-PCR assays. D.S. and S.B.D. prepared tissue samples for histological analysis and immunofluorescence imaging. M.B. and G.S. performed the statistical analyses. M.B., Z.Z., G.S. and G.P. wrote the manuscript.

Additional Information

Supplementary information accompanies this paper at <https://doi.org/10.1038/s41598-018-34582-6>.

Competing Interests: G.P., Z.G., and D.G. were shareholders in TavorStem Therapeutics, which provided no funding for this study.

Publisher's note: Springer Nature remains neutral with regard to jurisdictional claims in published maps and institutional affiliations.



Open Access This article is licensed under a Creative Commons Attribution 4.0 International License, which permits use, sharing, adaptation, distribution and reproduction in any medium or format, as long as you give appropriate credit to the original author(s) and the source, provide a link to the Creative Commons license, and indicate if changes were made. The images or other third party material in this article are included in the article's Creative Commons license, unless indicated otherwise in a credit line to the material. If material is not included in the article's Creative Commons license and your intended use is not permitted by statutory regulation or exceeds the permitted use, you will need to obtain permission directly from the copyright holder. To view a copy of this license, visit <http://creativecommons.org/licenses/by/4.0/>.

© The Author(s) 2018